Quantum Entanglement of One-Dimensional Spinless Fermions

A Thesis Presented

by

Emanuel Casiano-Diaz

to

The Faculty of the Graduate College

of

The University of Vermont

In Partial Fullfillment of the Requirements
for the Degree of Master of Science
Specializing in Physics

March 1st, 2019.

Defense Date: March 18nd, 2019.
Thesis Examination Commitee:

Adrian Del Maestro, Ph.D, Advisor
Dennis Clougherty, Ph.D
Christopher Danforth, Ph.D, Chairperson
Cynthia J. Forehand, Ph.D, Dean of the Graduate College

Abstract

The constituents of a quantum many-body system can be inextricably linked, a phenomenon known as quantum entanglement. Entanglement can be used as a resource for quantum computing, quantum communication and detecting phase transitions, among others. The amount of entanglement can be quantified via the von Neumann and Rényi entropies, which have their origins in information theory.

In this work, the quantum entanglement between subsystems of a one dimensional lattice model of fermions is quantified. The von Neumann and Rényi entropies were calculated for two types of subsystems. In the first study, the subsystems were treated as two subsets of particles, and in the second, as two spatial subregions. Finally, by considering particle conservation rules, the amount of entanglement that can actually be accessed as a resource was calculated. In all cases, the quantum entanglement served to detect phase transitions in the model.

Contents

Chapter 1

Introduction

1.1 The tV Model

So called "toy models" are ubiquitous in condensed matter physics. These describe a complex system in simple terms so that attention can be given to an underlying mechanism of such system. The Ising model, in it simplest form, can describe how a system spontaneously becomes a ferromagnet by considering interactions between quantum spins and tuning an external temperature. Similarly, the Hubbard model considers the interaction strength of electrons on a lattice and a hopping rate to describe the transition between conductor and insulator. The fact that the two aforementioned examples mention phase transitions is not mere coincidence.

Near a phase transition, evidence seems to point out to the fact that the behavior of a system is determine by a small set of parameters, a phenomenon known as universality. The size of a lattice could be one of these parameters, perhaps it could be the number of elements, or maybe even symmetry properties. Different systems having the same value for such universality parameters are said to fall under the same universality class.

This studies that will be presented in this thesis shall be concerned with a specific model, which shall be referred to as the tV model. The tV model describes N itinerant fermions on a 1D lattice of size L. These fermions can tunnel to neighboring sites and the rate at which they do so is proportional to a hopping parameter t. An interaction potential, V, between the fermions is also considered, which could be repulsive ($V > 0$) or attractive ($V < 0$). Periodic and anti-periodic boundary conditions will be assumed for the case of odd and even particles, respectively. Mathematically, this is represented by the following Hamiltonian:

$$H = -t \sum_i \left(c_i^\dagger c_{i+1} + c_{i+1}^\dagger c_i \right) + V \sum_i n_i n_{i+1} \tag{1.1}$$

where $c_i^\dagger$ (c_i) creates (annihilates) a fermion on site i and n_i counts the number of fermions on site i. In the case that there exists a fermion on site i already, then $c_i^\dagger = 0$ in order to satisfy Pauli's Exclusion Principle. The interaction term can then be understood conceptually as adding to the potential energy of the system if there are multiple particles in neighboring sites. Conceptually, the first term may be more difficult to understand in its current representation, due to this operator being non-diagonal. Nevertheless, expressing it in the momentum basis, which is diagonal, will illustrate that how contributions to the kinetic energy will come from

all particles with nonzero momentum (which will be all of them unless $t = 0$). A detailed mapping of the kinetic energy operator from lattice site to momentum basis can be seen in Appendix C.1.

test Eq. (1.1)

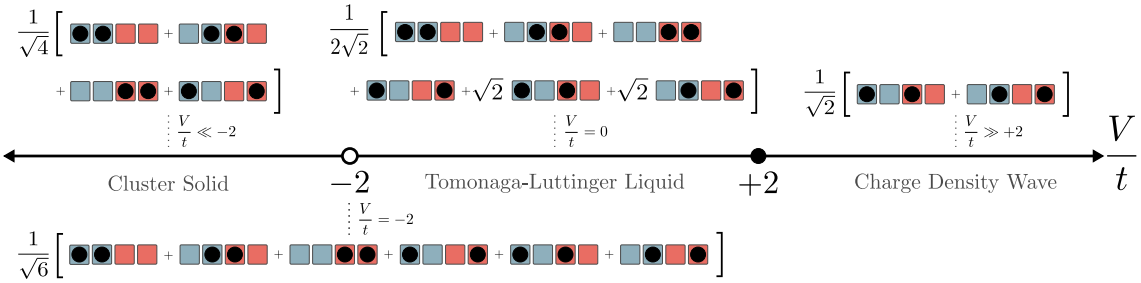

Figure 1.1: Phase diagram of the $t-V$ model accompanied by pictures of candidate ground states for $N = 2$ fermions on a $L = 4$ site lattice. For the purposes of measuring accessible entanglement, the lattice has been bipartitioned into spatial subregions A (blue) and B (red), each of size $\ell = 2$. We assume periodic boundary conditions. In the limit of strong attractive interactions where $V/t \ll -2$, the particles cluster together and there are L equally probable configurations corresponding to all translations of the cluster. At the first order phase transition where $V/t = -2$, all $\binom{L}{N}$ configurations are equally probable resulting in a flat state. In the TLL phase with $|V/t| < 2$, particles are delocalized and we have included a characteristic state corresponding to free fermions ($V = 0$). In the limit of strong repulsive interactions where $V/t \gg 2$, fermions maximize their distance from each other resulting in a charge density wave (CDW) phase. The open and closed circles on the V/t axis denote a first order and continuous phase transition, respectively.

Figure 1.1 shows the phase diagram of the tV model. For $V/t \ll -2$, the fermions cluster together due to the strong attractive interaction. The state in this regime is an equal superposition of all possible such cluster configurations over all lattice sites. At $V/t = -2$, the system undergoes a second order phase transition into the Tomonaga-Luttinger Liquid (TLL) phase. Here, the state is in a superposition of all possible configurations of the fermions on the lattice. The weights for these configurations are in general different and can only be exactly known at $V/t = 0$ [1]. At $V/t = 2$, the system undergoes a continuous phase transition into the charged density wave (CDW) phase. At $V/t \gg 2$, the strong repulsion between particles leads to them forming an alternating pattern of particle-vacancy-particle-vacancy ... The state in this regime becomes an equal superposition of the only two possible such configurations.

Notice that in Figure 1.1 the lattice sites have two different colors, blue and red. This is to illustrate that a system can be partitioned into smaller subregions. In this particular example, each partition would be of size 2 lattice sites. In fact, subdividing a system into this smaller subsystems will be necessary for the main phenomenon of interest in this thesis: quantum entanglement. The bulk of this work will consist on quantifying the amount of entanglement of a system via entropy measures. Before getting to explaining entanglement, in the next section, an overview of entropy or information measures will be given.

Chapter 2

Particle Partition Entanglement in the tV Model

2.1 Abstract

We investigate the scaling of the Rényi entanglement entropies for a particle bipartition of interacting spinless fermions in one spatial dimension. In the Tomonaga-Luttinger liquid regime, we calculate the second Rényi entanglement entropy and show that the leading order finite-size scaling is equal to a universal logarithm of the system size plus a non-universal constant. Higher-order corrections decay as power-laws in the system size with exponents that depend only on the Luttinger parameter. We confirm the universality of our results by investigating the one dimensional $t-V$ model of interacting spinless fermions via exact-diagonalization techniques. The resulting sensitivity of the particle partition entanglement to boundary conditions and statistics supports its utility as a probe of quantum liquids.

2.2 Introduction

Identical particles are fundamentally indistinguishable in quantum mechanics, unlike their classical counterparts that can always be discriminated due to an infinite set of observable properties. While this indistinguishability allows for the power provided by the second quantization formalism, it can also lead to ambiguity [2–4] when considering another defining property of composite quantum systems: entanglement. A pure state representing N quantum particles $|\Psi\rangle \in \mathcal{H}$ in Hilbert space $\mathcal{H}$ is said to be bipartite entangled if it cannot be written in a simple tensor product form $|\Psi\rangle \neq |\Psi_A\rangle \otimes |\Psi_B\rangle$ where A and B are vector spaces with $|\Psi_A\rangle \in A$ and $|\Psi_B\rangle \in B$ such that $A \otimes B = \mathcal{H}$. Conventionally, A and B correspond to a set of distinguishable single-particle modes whose occupation numbers are physical observables, i.e., spatial or momentum modes. However, for indistinguishable itinerant particles, there is no natural tensor product decomposition into single-particle modes due to the symmetrization or anti-symmetrization of the wavefunction with respect to the interchange of first quantized particle coordinates for bosons and fermions, respectively. Thus, the *mode entanglement* may depend on the choice of single-particle modes, leading to questions as to which (if any) are preferred and moreover, if these quantum correlations are even physically meaningful [5–12]. For example, even in

the absence of interactions, a system of N free itinerant bosons [13, 14] or fermions [15–17] is always entangled under a spatial biparition as a result of all allowed states being normalized linear combinations of Slater determinants or permanents.

Insights into these issues can be gained by considering the N-body wavefunction in first quantized form where a bipartition can be made in terms of identical particle labels. The resulting *n-particle partition entanglement* is a measure of quantum correlations between the subsets of n and $N-n$ particles. As individual (or groups of) identical particles are not operationally distinguishable, there have been claims that this type of entanglement is not useful as a resource for quantum information processing [5, 11, 18]. However, schemes have been recently proposed to transfer it to experimentally addressable modes [19]. In a foundational series of papers, Haque *et al.* explored the particle partition entanglement in fractional quantum hall [20, 21] and itinerant bosonic, fermionic and anyonic lattice gases in one spatial dimension [22, 23]. This type of particle partition entanglement has since been investigated in other one dimensional systems including the fermionic Calogero-Sutherland [24], anyonic hard-core [25] and bosonic Lieb-Liniger [26, 27] models as well as rotating bose and fermi gases in two dimensions [28]. In analogy to the universal finite size scaling behavior of the entanglement entropy of one dimensional quantum gases under a spatial mode bipartition [29–31], a leading order scaling form for the particle partition entanglement entropy S supported by exact diagonalization on small lattice models was proposed in Ref. [22] which is linear in the subsystem size n and logarithmic in the system size N: $S \sim n \ln N$.

Motivated by this empirical prediction, in this paper, we investigate the particle partition entanglement for itinerant interacting spinless fermions in one spatial dimension. For Galilean invariant systems in the spatial continuum, we confirm the scaling form proposed in Ref. [22] within the Tomonaga-Luttinger liquid framework [32, 33] and determine how the leading order power-law corrections to the asymptotic scaling depend on the strength of the interactions between particles for $n = 1$. By exploiting symmetries of the n-particle reduced density matrix, we are able to measure the particle entanglement entropy in the one dimensional fermionic $t-V$ model for systems composed of up to $M = 28$ lattice sites at half filling, allowing us to confirm our predictions from continuum field theory.

The rest of this paper is organized as follows. We introduce a quantitative measure of entanglement, the Rényi entanglement entropy and discuss some known results for interacting spinless fermions. We then derive the 1-particle entanglement entropy in the low energy limit and compare with exact diagonalization results on a lattice. We conclude with a discussion of the role of boundary conditions, degeneracy and implications for future studies of models with generalized statistics. All numerical data and code necessary to reproduce the results and figures in this paper can be found in Ref. [34].

2.3 Particle Partition Entanglement

The entanglement of the pure state $\left|\Psi\right\rangle$ under a general bipartition into A and B can be quantified via the Rényi entanglement entropy:

$$S_\alpha\left[\rho_A\right] \equiv \frac{1}{1-\alpha} \ln\left(\mathrm{Tr}\rho_A^\alpha\right), \tag{2.1}$$

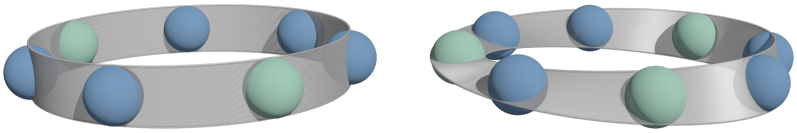

periodic: $N = 7,\ n = 2$ anti-periodic: $N = 8,\ n = 3$

Figure 2.1: A schematic of $N = 7$ fermions in one spatial dimension subject to periodic boundary conditions under a n-particle partition with $n = 2$ (left) and anti-periodic boundary conditions with $N = 8$ and $n = 3$ (right). All fermions are identical, while the partitions A and B are distinguished via their first quantized labels.

where α is the Rényi index and ρ_A is the reduced density matrix obtained by tracing out all degrees of freedom in B

$$\rho_A \equiv \mathrm{Tr}_B \left|\Psi\right\rangle\!\left\langle\Psi\right|. \tag{2.2}$$

For $\alpha = 1$ the Rényi entropy is equivalent to the von Neumann entropy: $-\mathrm{Tr}\ \rho_A \ln \rho_A$.

While it is common for A and B to be defined by some set of observable modes, for a many-body system consisting of N itinerant particles they can refer to subsystems of particles. As depicted in Fig. A.4, such a bipartition of indistinguishable particles (in this case spinless fermions) is completely specified by the number of particles in the subsystem, n. The entanglement entropy under a particle bipartition is then a function of the familiar n-body reduced density matrix ρ_n, (n-RDM) defined in first quantized notation in one spatial dimension as:

$$\rho_n \equiv \int dx_{n+1} \cdots \int dx_N \, \langle x_{n+1} \cdots x_N | \Psi \rangle \, \langle \Psi | x_{n+1} \cdots x_N \rangle \tag{2.3}$$

where we have taken the normalization $\mathrm{Tr}\rho_n = 1$. From this form, it is clear that the particle partition Rényi entropies $S_\alpha[\rho_n] \equiv S_\alpha(n)$ only vanish when the N-body ground state $\left|\Psi\right\rangle$ can be written as a general tensor product state in first quantized notation. This immediately implies that $S_\alpha(n) = 0$ when all particles are condensed into a single mode, and thus the particle partition entanglement of the non-interacting Bose gas is identically zero, in contrast to non-zero results for its spatial mode entanglement [13, 14]. This is not the case for many-fermion systems, which always have non-zero particle entanglement, even in the absence of interactions [16]. Particle entanglement entropy is sensitive to both interactions and statistics, and as ρ_n is free of any length scale, it can capture non-local effects making it complimentary to the more conventionally studied spatial mode entanglement entropy.

As described in the introduction, Zozulya et al. [22] first proposed a "standard" finite-size scaling form for the particle entanglement entropy of fermions:

$$S(n, N) = \ln \binom{N}{n} + a + \mathcal{O}\left(\frac{1}{N^\gamma}\right) \tag{2.4}$$

where a and γ are non-universal dimensionless numbers that can depend on n. These coefficients are known for the case of non-interacting fermions where $a = 0$ [23] and for the Laughlin state with filling fraction ν: $a = -n \ln \nu$, $\gamma = 2$ when $n \ll N$ [20].

Chapter 3

Operationally Accessible Entanglement Entropy in the tV Model

3.1 Operationally Accessible Entanglement Entropy

3.1.1 The Rényi Entanglement Entropy

The amount of entanglement that exists between some partition A and its compliment B of a quantum many-body system in pure state $|\Psi\rangle$ can be quantified via the Rényi entanglement entropy which depends on an index α :

$$S_\alpha(\rho_A) = \frac{1}{1-\alpha} \ln \operatorname{Tr} \rho_A^\alpha \tag{3.1}$$

where ρ_A is the reduced density matrix of partition A obtained by tracing out all degrees of freedom in B from the full density matrix:

$$\rho_A = \operatorname{Tr}_B \rho = \operatorname{Tr}_B |\Psi\rangle \langle\Psi| \ . \tag{3.2}$$

The Rényi entropy is a monotonically decreasing function of α for $\alpha > 1$ and is bounded from above by the von Neumann entropy, $S_1(\rho_A) = -\operatorname{Tr} \rho_A \ln \rho_A$.

For a quantum many-body system subject to physical laws conserving some quantity (particle number, charge, spin, etc.), the set of local operations on the state $|\Psi\rangle$ are limited to those that don't violate the corresponding global superselection rule. For the remainder of this paper, we will focus on our discussion on the case of fixed total N and thus we are restricted to only those operators which locally preserve the particle number in A. The effect this has on the amount of entanglement that can be transferred to a qubit register is apparent from the simple example (adapted from Ref. [8] of one particle confined to two spatial modes A and B corresponding to site occupations. Then, for the state $|\Psi\rangle = (|1\rangle_A \otimes |0\rangle_B + |0\rangle_A \otimes |1\rangle_B)/\sqrt{2}$, Eq. (3.1) gives that $S_1 = \ln 2$. However, this entanglement cannot be transferred to a register prepared in initial state $|0\rangle_R$ via a `SWAP` gate:

$$\begin{aligned} &\texttt{SWAP}\, |0\rangle_R \otimes (|1\rangle_A \otimes |0\rangle_B + |0\rangle_A \otimes |1\rangle_B)/\sqrt{2} \\ &= \frac{1}{\sqrt{2}} (|0\rangle_R \otimes |0\rangle_A \otimes |1\rangle_B + |1\rangle_R \otimes |0\rangle_A \otimes |0\rangle_B) \end{aligned}$$

entanglement for this state is dependent on the parity of the total number of particles N. Up next, the result for even N will be derived.

3.3.1.1 Even N

In the following calculations, the system will be partitioned into spatial subregions A and B, both containing the same number of sites. In other words, if the total number of sites in the $t-V$ chain is L, then the partition size will be $l = \frac{L}{2}$.

In the case of even particle number N, the CDW state will have the same number of particles in each subregion A and B:

$$|\Psi\rangle_{N_{Even}} = \frac{1}{\sqrt{2}}[|\underbrace{1010...}_{\frac{N}{2}particles}, \underbrace{1010...}_{\frac{N}{2}particles}\rangle + |\underbrace{0101...}_{\frac{N}{2}particles}, \underbrace{0101...}_{\frac{N}{2}particles}\rangle] \tag{3.20}$$

As a reminder, labels left to the comma correspond to spatial subregion A, while those to the right correspond to B.

The full density matrix ρ_{AB} takes the form:

$$\begin{aligned}\rho_{AB} &= |\Psi\rangle_{N_{Even}}\langle\Psi|_{N_{Even}} \\ &= \frac{1}{2}|0101..., 0101\rangle\langle 0101..., 0101...| + \frac{1}{2}|0101..., 0101\rangle\langle 1010..., 1010...| \\ &+ \frac{1}{2}|1010..., 1010\rangle\langle 0101..., 0101...| + \frac{1}{2}|1010..., 1010\rangle\langle 1010..., 1010...|\end{aligned} \tag{3.21}$$

Recall that to calculate the entanglement entropies, it is necessary to obtain the reduced density matrix of subsystem A. Taking the partial trace with respect to B, the reduced density matrix of A is obtained:

$$\rho_A = \mathrm{Tr}_B\, \rho_{AB} \quad = \sum_n {}_B\langle n|\Psi\rangle\langle\Psi|n\rangle_B \tag{3.22}$$

The summation above is carried over all possible states that B can be found in. In this case, there are only two possible B states: $n = |0101...\rangle_B$ and $n = |1010...\rangle_B$. Thus, taking the partial trace respect to B of 3.21, the reduced density matrix of A becomes:

$$\rho_A = \frac{1}{2}(|0101...\rangle_A\langle 0101...|_A + |1010...\rangle_A\langle 1010...|_A]) \tag{3.23}$$

Notice that some of the terms have vanished due to the orthonormality of the states. At this point, it will be convenient for purposes of illustration to rewrite the reduced density matrix of A in actual matrix form rather than in Dirac or Bra-Ket notation. Following the convention $|0101\ldots\rangle_A$ and $|1010\ldots\rangle_A$ for columns and rows from left to right and top to bottom, respectively, the reduced density matrix of A can be written as:

$$\begin{aligned}\rho_{AB} &= |\Psi\rangle_{N_{Odd}}\langle\Psi|_{N_{Odd}} \\ &= \frac{1}{2}(|...101,010...\rangle\langle...101,010...| + |...101,010...\rangle\langle...010,101...| \\ &+ |...010,101...\rangle\langle...101,010...| + |...010,101...\rangle\langle...010,101...|)\end{aligned} \tag{3.27}$$

The possible B states are: $n = |101...\rangle, |010...\rangle$ with $\frac{N+1}{2}$ and $\frac{N-1}{2}$ particles, respectively. Taking the partial trace respect to B, the reduced density matrix of A becomes:

$$\rho_A = \frac{1}{2}(|101...\rangle_A\langle 101...|_A + |010...\rangle_A\langle 010...|_A) \tag{3.28}$$

Once again, it may be more illustrative to rewrite in matrix form. Defining an orthonormal basis $|101...\rangle_A = \begin{pmatrix}1\\0\end{pmatrix}$ and $|010...\rangle_A = \begin{pmatrix}0\\1\end{pmatrix}$ the reduced density matrix of A becomes:

$$\rho_A = \begin{pmatrix}\frac{1}{2} & 0\\ 0 & \frac{1}{2}\end{pmatrix} \tag{3.29}$$

The simple projection operators onto $\frac{N+1}{2}$ and $\frac{N-1}{2}$ particle space in this basis are:

$$\mathcal{P}_{A_{\frac{N+1}{2}}} = \begin{pmatrix}1 & 0\\ 0 & 0\end{pmatrix}, \mathcal{P}_{\frac{N-1}{2}} = \begin{pmatrix}0 & 0\\ 0 & 1\end{pmatrix} \tag{3.30}$$

Applying these projections to ρ_A and choosing the probability such that the trace of each matrix is unity (normalization), the projected reduced density matrices become:

$$\rho_{A_{\frac{N+1}{2}}} = \begin{pmatrix}1 & 0\\ 0 & 0\end{pmatrix} \text{ with probability } P_{\frac{N+1}{2}} = \frac{1}{2} \tag{3.31}$$

and

$$\rho_{A_{\frac{N-1}{2}}} = \begin{pmatrix}0 & 0\\ 0 & 1\end{pmatrix} \text{ with probability } P_{\frac{N-1}{2}} = \frac{1}{2} \tag{3.32}$$

Substituting into the accessible entanglement equation (3.18):

$$\begin{aligned}S_\alpha^{acc}(\rho_A) &= \sum_n P_n S_\alpha(\rho_{A_n}) \\ &= (\frac{1}{2})\frac{1}{1-\alpha}\ln \mathrm{Tr}\left\{\rho^\alpha_{A_{\frac{N+1}{2}}}\right\} + (\frac{1}{2})\frac{1}{1-\alpha}\ln \mathrm{Tr}\left\{\rho^\alpha_{A_{\frac{N-1}{2}}}\right\} \\ &= \frac{1}{2-2\alpha}[\ln \mathrm{Tr}\left\{\begin{pmatrix}1^\alpha & 0\\ 0 & 0\end{pmatrix}\right\} + \ln \mathrm{Tr}\left\{\begin{pmatrix}0 & 0\\ 0 & 1^\alpha\end{pmatrix}\right\}] \\ &= \frac{1}{2-2\alpha}[\underbrace{\ln 1 + \ln 1}_{=0}] \\ S_\alpha^{acc}(\rho_A) &= 0\end{aligned} \tag{3.33}$$

Therefore, the accessible entanglement vanishes in the infinite repulsion limit ($V/t \to +\infty$) with odd number of total particles in the system.

Interaction	$\frac{\alpha}{1-\alpha}\ln\left[\sum_n P_n \mathrm{e}^{\frac{1-\alpha}{\alpha}S_\alpha(\rho_{A_n})}\right]$	$\sum_n P_n S_\alpha(\rho_{A_n})$
$V/t \to -\infty$	$\frac{\alpha}{1-\alpha}\left[\frac{2(x-1)}{L}2^{\frac{1-\alpha}{\alpha}} + 1 - \frac{2(x-1)}{L}\right]$	$\frac{2(x-1)}{L}\ln 2$
$V/t \to +\infty$	$\ln 2$ if N even, 0 if N odd	$\ln 2$ if N even, 0 if N odd
$V/t = -2$	0	0

Table 3.1: Analytical results for the accessible entanglement in the ground state of the tV model with N fermions on L sites under a spatial bipartition consisting of $\ell = L/2$ contiguous sites. From left to right, the columns indicate the interaction strength, the value of the generalized Rényi accessible entanglement, and the value of the traditional entanglement, respectively. The x in the first row is the minimum value between $\{N, \ell, L-\ell, L-N\}$.

the tV model. For large negative interaction strengths, there is agreement between the values at which $S_\alpha^{\mathrm{acc}}(\rho_A)$ converges and the predicted value from 3.1 for all system sizes and α. For large positive interaction strengths, the predicted effect of total particle number parity is observed. For N odd, the accessible entanglement vanishes, whereas it converges to $\ln 2 \approx 0.6931\ldots$ for N even, independent of system size and α. At the first order phase transition $V/t = -2$, $S_\alpha^{\mathrm{acc}}(\rho_A)$, as expected. Thus, the asymptotic predictions for the accessible entanglement entropy in the tV model have been confirmed via exact diagonalization. Increasing the magnitude of both the attractive and repulsive interactions will result in even more agreement between simulation and theory.

Recall that the accessible entanglement should be a monotonically decreasing function of α. Figure 3.1 supports this inverse relation since it is seen that $S_1 \geq S_2$ $\forall\ V/t \in (-100, 100)$.

Another interesting feature is the peak seen near the continuous phase transition $V/t = 2$. Results seem to indicate that the peak is slightly shifting to the left, closer to $V/t = 2$ as the number of particles N increases. In an effort to find how the location of this peak scales with particle number, $V/t|_{Max}$ was obtained for various system sizes, where $V/t|_{Max}$ is the interaction strength at which the accessible entanglement peak occurs. Figure 3.2 shows a plot of $V/t|_{Max}$ vs $N^{-0.3066}$. The exponent comes from a linear fitting of $(V/t|_{Max} - 2)$ vs N data. The observed inverse power law scaling is promising as all points fall on a line with y intercept of $V/t|_{Max} = 2$, which is the exact value of the continuous phase transition in the asymptotic limit of $N \to \infty$ total particles.

3.5.2 Entanglement of local particle number fluctuations

Recall from section 3.1.1 that the difference between the full and the operationally accessible entanglement von Neumann entropies ($\alpha = 1$) should equal the Shannon Entropy of the local particle number probability distribution P_n:

$$\Delta S_1(\rho_A) \equiv S_1(\rho_A) - S_1^{\mathrm{acc}}(\rho_A) = H_1(\{P_n\}) \tag{3.68}$$

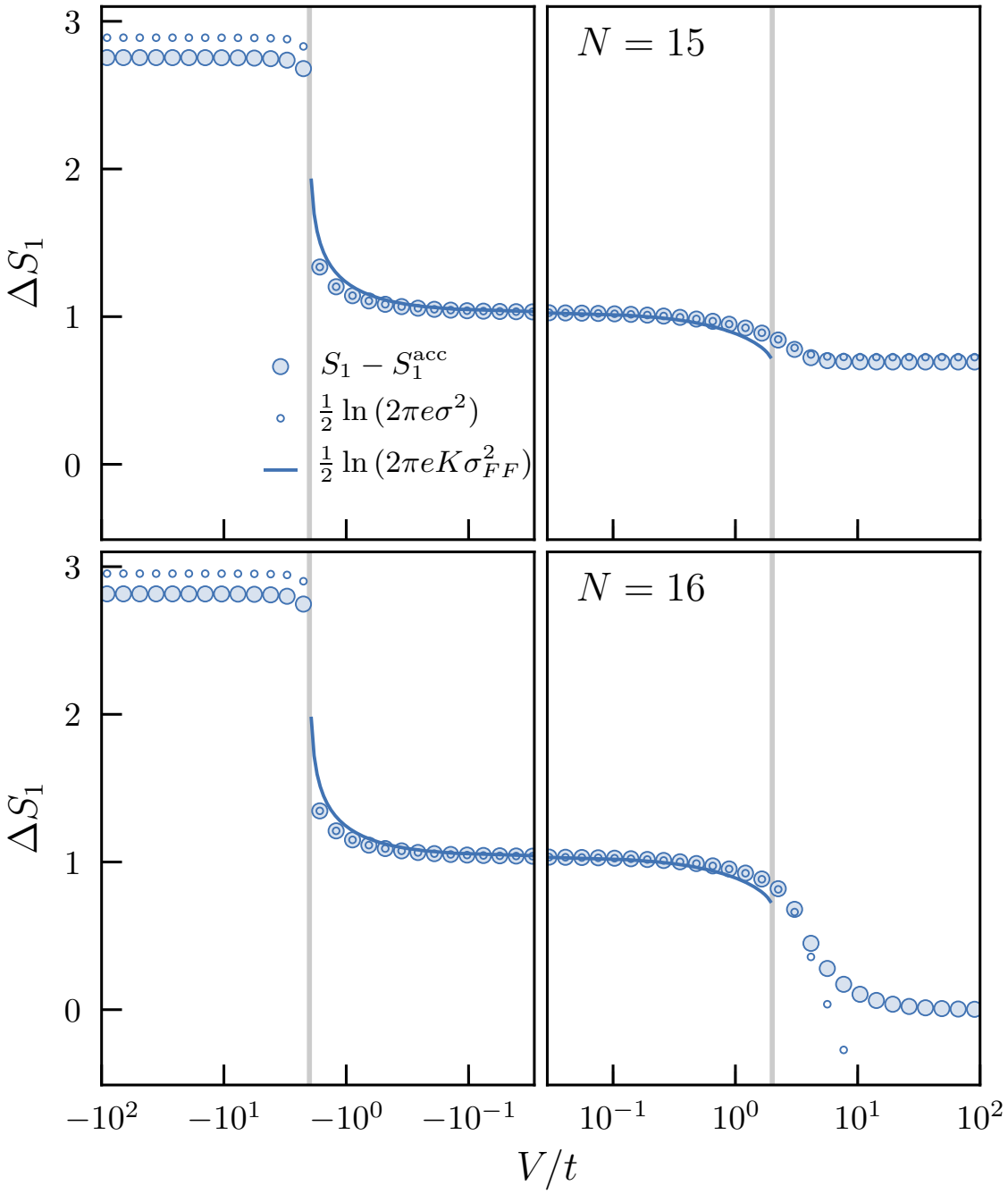

Figure 3.3: Difference between the von Neumann and accessible entanglement entropies $S_1 - S_1^{acc}$ and $\frac{1}{2}\ln 2\pi e\sigma^2$ as functions of interaction strength V/t. The latter expression is the well known differential entropy of a Gaussian distribution. In TLL phase ($-2 < V/t < 2$), the probability distribution is Gaussian, as can be seen from the agreement between the two results. The solid lines use the theoretical variance of particle number in A inside the LL phase, $K\sigma_{FF}^2$, where K is the Luttinger parameter and is a function of V/t and σ_{FF}^2 is the exact variance for free-fermions ($V/t = 0$).

Notice that raising Eq. 3.71 to either $1/\alpha$ or K on both sides should get rid of the α or K dependence of the exponential factor, respectively, within the TLL regime. The square root factor will still pick up the dependence on either of the exponents. In other words, raising by $1/\alpha$ or K should give:

$$P_{n,\alpha}^{1/\alpha} \approx \sqrt{\frac{\pi\alpha}{2K\ln\ell}}^{1/\alpha} e^{\frac{-\pi^2(n-\langle n\rangle^2)}{2K\ln\ell}} \tag{3.72}$$

and

$$P_{n,\alpha}^{K} \approx \sqrt{\frac{\pi\alpha}{2K\ln\ell}}^{K} e^{\frac{-\alpha\pi^2(n-\langle n\rangle^2)}{2\ln\ell}} \tag{3.73}$$

Figure 3.6 shows the distribution $A_\alpha P_{n,\alpha}^{1/\alpha}$ for various interaction strengths V/t and, thus, K. The constant A_α is the inverse of the square root factor in Eq. 3.72. Cancelling the square root factor allows for a direct comparison of the exponential factor for each of the α values used. The middle plots confirm that this exponential factor indeed is independent of α, illustrated by the fact that the distributions become the same for $\alpha = \{1, 2, 5, 10\}$, when inside the TLL regime of $-2 < V/t < 2$.

Figure 3.7 shows the distribution $A_\alpha P_{n,\alpha}^{K}$ with the Rényi index fixed at $\alpha = 2$ and at various interaction strengths V/t and corresponding Luttinger parameters K. In this case, the factor A_α is the inverse of the square root factor in Eq. 3.73. All of the interaction strengths fall within the TLL regime and as such, all the distributions should become the same for the various V/t and, thus, K values. This collapse of the distributions at various K is evident from looking at regions near the middle of the graph. Although it may not be apparent at first glance due to the scale, the tails of the distribution are all essentially zero.

3.6 Conclusion

In this chapter, the operationally accessible Rényi entanglement entropy was introduced in both it's original and generalized form. Analytical values of the entanglement entropy were obtained at various special cases of the tV model and then confirmed via exact diagonalization. A maximum value in accessible entanglement was observed and evidence seems to support that it follows an inverse power law scaling in total particle number with scaling exponent of -0.3066.

The difference in full and accessible entanglement entropies was also computationally determined and it was confirmed that in the TLL phase of the tV model, it is equal to the the Rényi entropy of a Normal Distribution of local particle number. Finally, it was then proposed theoretically and confirmed computationally, that getting rid of its Rényi index and Luttinger parameter dependence, the exponential part of these Normal Distributions depend exclusively on local particle number fluctuations.

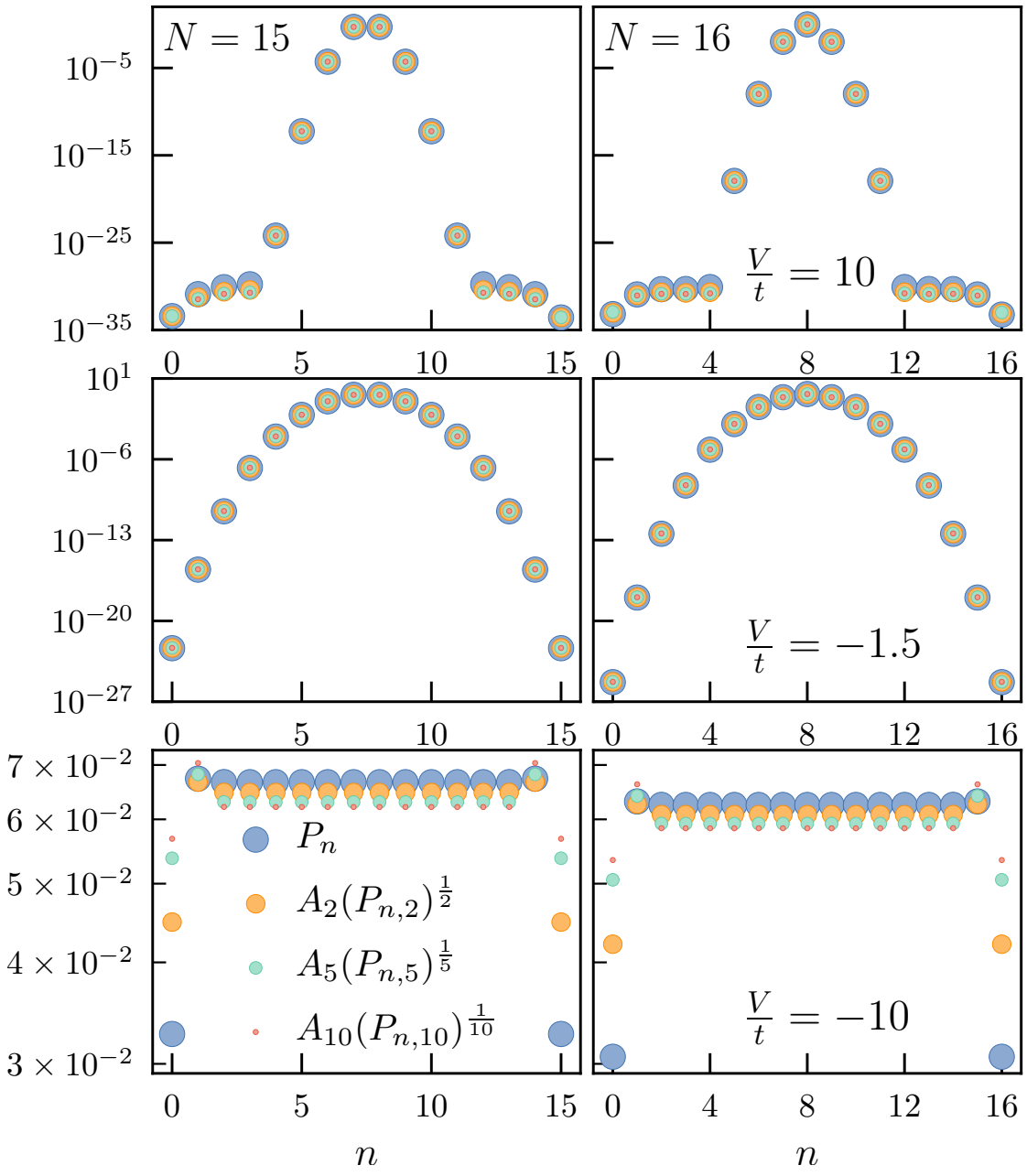

Figure 3.6: Probabilities of measuring a state with n particles in subregion A, as a function of n. The probabilities in the TLL regime are known to be Gaussian, as seen from Eq.6. Here, they have been raised to $1/\alpha$ in order to cancel out the α dependence of the exponential part. For the middle plot, the interaction strength lies in the TLL regime and, consequently, the probabilities collapse to the same values in all the range after the α dependence has been cancelled. The top and bottom plots show results outside of the TLL regime, where the probabilities are not Gaussian.

Appendix A

Appendix

A.1 Lanczos Algorithm

A.1.1 Introduction

The Lanczos Algorithm, takes as input a Hermitian Matrix and iteratively builds a similarity transform that makes it tridiagonal. Due to similarity, the solution of the eigenvalue problem of the tridiagonal matrix is the same as that of the original matrix. Nevertheless, some methods can exploit the tridiagonality to find the eigendecompositio more easily. In condensed matter physics, the input matrix is usually a Hamiltonian. The eigenvalues and eigenvectors of the Hamiltonian represent the energies and the associated quantum states of the system.

In the following section, the Lanczos Algorithm will be derived. Next, some methods for approximating the eigenvalues and eigenvectors will be discussed. Finally, a hopefully simple implementation of the algorithm in Python will be linked and some results will be shown.

A.1.2 Tridiagonalization of the original matrix

Let A be a Hermitian matrix of size nxn. An orthonormal transform matrix Q is needed such that:

$$T = Q^T A Q$$

where T is a tridiagonal and Hermitian matrix similar to A.

The idea is to obtain a recursive relation, starting from the known fact that T is tridiagonal and that the columns of the transform Q are mutually orthonormal. The matrix T has the form:

$$T = \begin{pmatrix} \alpha_1 & \beta_1 & & & & & 0 \\ \beta_1 & \alpha_2 & \beta_2 & & & & \\ & \beta_2 & \alpha_3 & \beta_3 & & & \\ & & \beta_3 & \ddots & \ddots & & \\ & & & \ddots & \alpha_{n-2} & \beta_{n-2} & \\ & & & & \beta_{n-2} & \alpha_{n-1} & \beta_{n-1} \\ 0 & & & & & \beta_{n-1} & \alpha_n \end{pmatrix}$$

$$q_{k+1} = \frac{r_k}{\beta_k} \tag{A.5}$$

where $\beta_k \neq 0$ and, since q_{k+1} is an orthonormal vector, $\beta_k = ||r_k||_2$, such that q_{k+1} is normalized.

Note that the α_k and β_k terms of the three-term recursion relation have been accounted for. As for the β_{k-1}, a "bottom rung" for the recursion has to be set. The tridiagonal matrix T does not have a β_{k-1} term. Thus, for $k = 1$, the $\beta_{k-1}q_{k-1}$ term is set to $\beta_0 q_0 = 0$. Now the columns of Q can be built by iterating from $k = 1$ to $k = n$.

A.1.3 Algorithm

1. Set $r_0 = q_1$,$\beta_0 = 1$ and $q_0 = 0$
2. For k=1,2,3,...,n:
3. $q_{k+1} = \frac{r_k}{\beta_k}$
4. $\alpha_k = q_k^T A q_k$
5. $r_k = (A - \alpha_k I)q_k - \beta_{k-1}q_{k-1}$
6. $\beta_k = ||r_k||_2$
7. Reorthonormalize $\{q_i\}_{i=1}^k$ if necessary
8. Approximate Eigenvalues and Eigenvectors (Can be done after the loop instead)

Line 1: β_0 is set to 1 since it is the norm of r_0 and $r_0 = q_1$, where q_1 is a normalized vector.

Line 2: The for loop runs from $k = 1$ all the way up to $k = n$, where n is the total number of columns. Depending of the eigenvalues desired, this loop can instead be a while loop that ends whenever the eigenvalues have reached a desired tolerance.

Line 7: Due to finite precision errors, the set of supposedly mutually orthonormal vectors $\{q_i\}_{i=1}^k$ will actually lose their orthonormality at later Lanczos steps. When this happens, a reorthonormalization scheme, such as the Grahm-Schmidt Process, has to be employed.

Line 8: Again, depending on the problem and the desired eigenpairs, the approximation can be done for the current version of the tridiagonal matrix at step k, call it T_k. Alternatively, it could be done after the for loop has finished and the full tridiagonal matrix has been T built. There is no strict requirement on which iterative method should be used to find the eigendecomposition (QR Method, Power Iteration, Inverse Power Iteration, etc...).

A.1.4 Code

An implementation of the Lanczos Algorithm in Python can be found in: https://github.com/ecasian
The code generates a random, sparse, hermitian matrix of specified size, finds a tridiagonal representation via Lanczos and calculates the full eigendecomposition via QR Algorithm or finds the smallest eigenvalue via Inverse Power Iteration. A blackbox

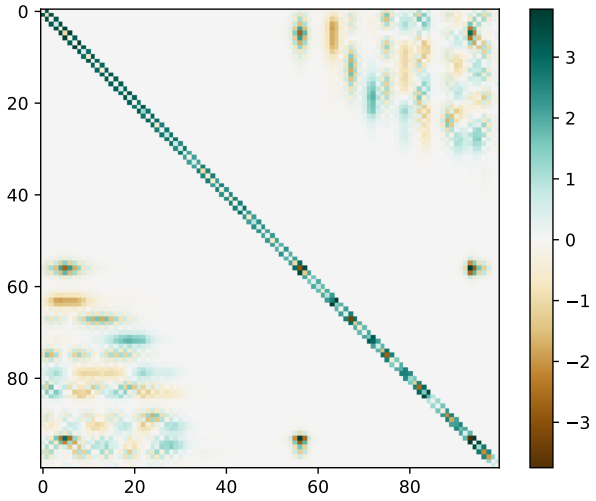

Figure A.2: INSERT CAPTION.

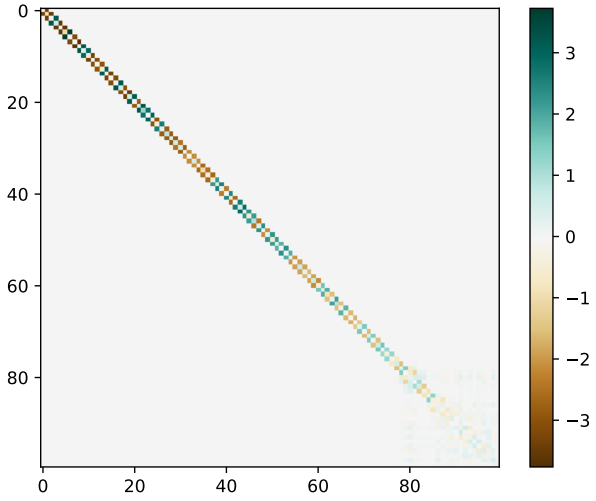

Figure A.3: INSERT CAPTION.

Bibliography

[1] H. Barghathi, C. M. Herdman, and A. Del Maestro. "Rényi generalization of the accessible entanglement entropy." Phys. Rev. Lett. **121**, 150501 (2018). https://link.aps.org/doi/10.1103/PhysRevLett.121.150501

[2] P. Zanardi. "Virtual Quantum Subsystems." Phys. Rev. Lett. **87**, 077901 (2001).

[3] Y. Shi. "Quantum entanglement of identical particles." Phys. Rev. A **67**, 024301 (2003).

[4] Y. Shi. "Quantum entanglement in second-quantized condensed matter systems." J. Phys. A: Math. Gen **37**, 6807 (2004).

[5] G. Ghirardi and L. Marinatto. "General criterion for the entanglement of two indistinguishable particles." Phys. Rev. A **70**, 012109 (2004).

[6] H. Barnum, E. Knill, G. Ortiz, R. Somma, and L. Viola. "A Subsystem-Independent Generalization of Entanglement." Phys. Rev. Lett. **92**, 107902 (2004).

[7] J. Dunningham, A. Rau, and K. Burnett. "From Pedigree Cats to Fluffy-Bunnies." Science **307**, 872 (2005).

[8] H. M. Wiseman, S. D. Bartlett, and J. A. Vaccaro. "Ferreting out the fluffy bunnies: entanglement constrained by generalized superselection rules." In "Proceedings of the XVI International Conference on Laser Spectroscopy," pages 307–314 (World Scientific, Queensland, Australia, 2011). https://www.worldscientific.com/doi/abs/10.1142/9789812703002_0047

[9] H. M. Wiseman and J. A. Vaccaro. "Entanglement of Indistinguishable Particles Shared between Two Parties." Phys. Rev. Lett. **91**, 097902 (2003).

[10] F. Benatti, R. Floreanini, and U. Marzolino. "Entanglement robustness and geometry in systems of identical particles." Phys. Rev. A **85**, 042329 (2012).

[11] A. P. Balachandran, T. R. Govindarajan, A. R. de Queiroz, and A. F. Reyes-Lega. "Entanglement and Particle Identity: A Unifying Approach." Phys. Rev. Lett. **110**, 080503 (2013).

[12] B. J. Dalton, J. Goold, B. M. Garraway, and M. D. Reid. "Quantum entanglement for systems of identical bosons: I. general features." Phys. Scrip. **92**, 023004 (2017).